Accepted Manuscript

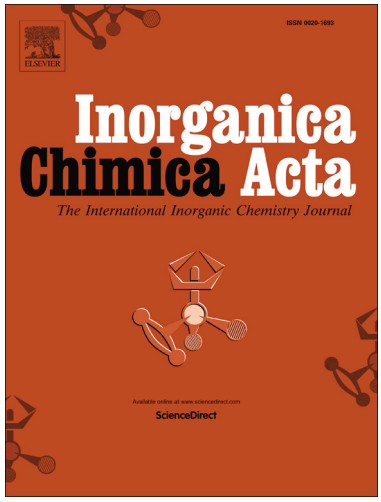

Research paper

Pyridoxal derivatized copper(II) complexes: Evaluation of antioxidant, catecholase, and DNA cleavage activity.

Mateus Brum Pereira, Liniquer Andre Fontana, Josiéli Demetrios Siqueira, Bruna L. Auras, Marcos P. da Silva, Ademir Neves, Philipe Gabriel, Hernán Terenzi, Bernardo Almeida Iglesias, Davi Fernando Back

PII: S0020-1693(17)30615-1
DOI: https://doi.org/10.1016/j.ica.2017.09.063
Reference: ICA 17922

To appear in: *Inorganica Chimica Acta*

Received Date: 24 April 2017
Revised Date: 7 July 2017
Accepted Date: 29 September 2017

Please cite this article as: M.B. Pereira, L.A. Fontana, J.D. Siqueira, B.L. Auras, M.P. da Silva, A. Neves, P. Gabriel, H. Terenzi, B.A. Iglesias, D.F. Back, Pyridoxal derivatized copper(II) complexes: Evaluation of antioxidant, catecholase, and DNA cleavage activity., *Inorganica Chimica Acta* (2017), doi: https://doi.org/10.1016/j.ica.2017.09.063

Pyridoxal derivatized copper(II) complexes: Evaluation of antioxidant, catecholase, and DNA cleavage activity.

Mateus Brum Pereira[a], Liniquer Andre Fontana[a], Josiéli Demetrios Siqueira[a], Bruna L. Auras[b], Marcos P. da Silva[b], Ademir Neves[b], Philipe Gabriel[c], Hernán Terenzi[c], Bernardo Almeida Iglesias[a] and Davi Fernando Back*[a]

[a]*Departamento de Química, Laboratório de Materiais Inorgânicos, Universidade Federal de Santa Maria, UFSM, 97115-900 Santa Maria - RS, Brazil.*

[b]*Departamento de Química, Universidade Federal de Santa Catarina, Florianópolis, SC 88040-900, Brazil.*

[c]*Centro de Biologia Molecular Estrutural,* Departamento de Bioquímica, Universidade *Federal de Santa Catarina, Florianópolis, SC 88040-900, Brazil.*

ABSTRACT

This manuscript describes the synthesis, characterization and structural analysis of copper(II) complexes with pyridoxal-type bidentate ligands, obtained from the condensation between pyridoxal and *ortho*-halogenated substituted anilines (**C1-C5**). The complexes **C1**, **C2** and **C5** were measured by X-ray single crystal analysis which showed classic and trifurcated hydrogen bonds and interaction as a sigma-hole between the oxygen atoms of the iodine ligand derivative in the complex **C5**. All compounds were tested as mimetics of superoxide dismutase (SOD), through NBT photoreduction method in aqueous solution of pH 7.8, but the complex **C5** showed an expressive IC_{50} of 0.4μM.

In addition, catecholase-like activity of **C1-C5** in the presence of the substrate 3,5-di-tert-butylcatechol and cleavage of plasmid DNA were also evaluated. Again, the best results were associated with the complex **C5** containing iodine in the *ortho* position.

Keywords: *Pyridoxal Schiff bases; copper(II) complexes; SOD mimetics, catecholase activity, plasmid DNA cleavage.*

1. INTRODUCTION

Pyridoxal acts as a coenzyme and many studies have demonstrated their performance in amino acid biosynthesis in transamination and decarboxylation, as well as in racemization processes. In biological systems, after conversion to pyridoxal-5'-phosphate, pyridoxine is incorporated into a variety of enzymes that catalyze these reactions [1,2]. When the pyridoxal unit is derivatized (mainly involving condensation reactions) Schiff-base ligands are obtained. There are numerous examples in the literature that illustrate the coordination with uranium, vanadium [3-5], iron, nickel, cobalt [6-8] and palladium [10], as well as *p*-block metals such as tin [9]. However, to date, there are only a few reports about the applicability of complexes involving the pyridoxal moiety and its antioxidant activity, specifically mimetics of superoxide dismutase (SOD) [11]. This group of enzymes can catalyze the dismutation of the superoxide anion, converting it into oxygen and hydrogen peroxide [12]. In the human body these types of antioxidant enzymes are divided into those that exhibit Cu/Zn or Mn metal ion centers [13-14].

There is also a lack of information in the literature about pyridoxal complexes with the potential to bind and cleave nucleic acids. Even though interaction of DNA with complexes of many transition metal ions has been investigated [15], copper(II) complexes are the preferred molecules for bringing about DNA cleavage. This is due to the fact that copper(II) complexes can bring about not only oxidative DNA cleavage, but also hydrolytic, photolytic or electrolytic cleavage [16-19]. Copper(II) complexes are also reported in the literature as potential antioxidant [20-22] antitumor, antimicrobial and anti-inflammatory molecules [23].

In this context, this study aimed to synthesize and characterize copper(II) complex derivatives from pyridoxal and *ortho*-substituted haloanilines and evaluate them with regard to potential as SOD biomimetics (SOD-1), catecholase activity and interaction with plasmid DNA.

2. EXPERIMENTAL

2.1. General Instrumentation

All manipulations were conducted by use of standard argon atmosphere. CHN% elemental analyses were performed at a Shimadzu EA112 microanalysis instrument. Compounds were analyzed using a mass spectrometer with electrospray ionization (ESI-MS) in the positive mode using an Amazon X Ion Trap (Bruker Daltonics, Billerica, MA). Mass spectra were recorded with the methanolic solutions of around 500 ppb concentration with a flow of 180 µL/min and capillary of 3500 V. High resolution ESI-MS (HRMS-ESI) was performed on a micrOTOF QII mass spectrometer (Bruker Daltonics, Billerica, MA). IR spectra were recorded on a Tensor 27 Bruker spectrometer with KBr pellets in the 4000-400 cm^{-1} region. UV-vis spectra were recorded on a UV-2600 Shimadzu spectrometer. Cyclic voltammograms were recorded with an EcoChemie PGSTAT 32N system at room temperature and under argon atmosphere, in dry acetonitrile solution. Electrochemical grade tetrabutylammonium hexafluorophosphate ($TBAPF_6$) was used as supporting electrolyte (0.1 mol/L acetonitrile solution). These CV experiments were carried out by employing a standard three-component system: a glassy carbon working electrode; a platinum wire auxiliary electrode and a platinum wire *pseudo*-reference electrode. To monitor the reference electrode, the ferrocenium/ferrocene couple was used as an internal reference [24].

2.2. X-Ray crystallography

Data were collected on a Bruker D8 Venture Photon 100 diffractometer equipped with an Incoatec IμS high brilliance Mo Kα X-ray tube with two-dimensional Montel micro-focusing optics. The structure was solved by direct methods using SHELXS [25]. Subsequent Fourier-difference map analyses yielded the positions of the non-hydrogen atoms. Refinements were carried out with the SHELXL package [25]. All refinements were made by full-matrix least-squares on F^2 with anisotropic displacement parameters for all non–hydrogen atoms. Hydrogen atoms were included in the refinement in calculated positions but the atoms (of hydrogens) that are commenting performing special bond were located in the Fourier map. Drawings were done using *DIAMOND* for Windows [26]. Crystal data and more details of the data collection and refinements of the complexes **C1, C2** and **C5** are presented in **Table 1**.

2.3. DNA Cleavage assays

The plasmid pBSK-II (Stratagene, USA) was used in the cleavage tests. This plasmid was produced in *Escherichia coli* DH5-α, following the protocol recommended by Ausubel and co-workers [27] and described in detail by Oliveira and collaborators [28]. DNA was extracted and purified following the protocol for extraction and purification of plasmid DNA (HiSpeed Plasmid Maxi Kit-Qiagen). The extracted plasmid DNA concentration was quantified using UV spectrophotometry and its integrity verified by agarose gel electrophoresis [27,28].

A typical cleavage reaction (20 µL) contained 330 ng of DNA pBSK II, buffered with 10 mM HEPES (pH 7.0) and treated with complexes at various concentrations. The reaction time was 16 hours at 37 ºC. During the reaction, the samples were kept sheltered from light. To interrupt the cleavage reactions, 5 µL of sample buffer (0.25 M EDTA, pH 8.0, 50% glycerol and 0.01% bromophenol blue) were added. The samples were then kept refrigerated (4ºC) until subjected to 1% agarose gel electrophoresis, containing ethidium bromide (0.3 µg/mL) for 100 minutes at 90 V with TBE 0.5X running buffer (44.5 mM Tris, 44.5 mM boric acid and 1 mM EDTA at pH 8.0). The gels were documented using a DigiDoc-It (UVP, USA) system and the fraction of each plasmid DNA form quantified by densitometry, using KODAK Molecular Imaging Software 5.0 (Carestream Health, USA). Since ethidium bromide intercalates to a lesser extent to the supercoiled form of the plasmid DNA, a correction factor of 1.47 was used when measuring this topological form of plasmid DNA [29].

2.4. ROS scavenger's effect

DNA cleavage can occur by, at least, two distinct mechanisms: hydrolytic or oxidative [30]. To evaluate the nature of such cleavage mechanisms, experiments were conducted in the presence of reactive oxygen species scavengers, such as 0.5 mM KI, a peroxide generation inhibitor; and 0.5 mM NaN_3, a singlet oxygen scavenger species ($^1O_2$).

2.5. DNA groove binders: effect on DNA cleavage

To determine the interaction specificity for the minor or major DNA grooves during the cleavage process, two small molecules known for binding with each groove were alternately added 30 minutes before the addition of complex, being them netropsin, a classical minor groove binder [31], and methyl green, a major groove binder [32].

2.6. DNA cleavage kinetics assays

Cleavage kinetics experiment is a key point to compare the efficiency of different catalyzers. The assays were performed using a final volume of 120 µL, to which 2 µg of plasmid DNA in 10 mM HEPES (pH 7.0) were added, followed by 30 µL of copper(II) complex (250 µM). Aliquots of 20 µL were taken at different times (0, 2, 4, 8 and 24 hours) and subjected to agarose gel electrophoresis. Cleavage kinetic constants (k_{obs}) were estimated for each specific concentration, taking these reactions as *pseudo* first-order. The value of k_{obs} was obtained directly from the angular coefficient of the linear regressions attained from the plot of the natural logarithm of the quantity of DNA versus reaction time.

2.7. Thermal denaturation with CT-DNA

Calf-Thymus DNA denaturation can be detected by the raising on light absorption (hyperchromic effect) [33]. The needed temperature to denature half of the DNA molecules is called denaturation mean temperature (T_m). When a molecule interacts with DNA the T_m can be altered. Based on such concepts, the T_m of CT-DNA was calculated in the absence or presence of the most active complex. The assays were performed in a UV-Visible Ultrospec 2100 spectrophotometer (Amersham Biosciences, USA). CT-DNA solution (50 µM) untreated or treated with complex (5 µM) remained 10 minutes at the initial start temperature (40 ºC). The temperature was then raised by 1 ºC / minute until 90 ºC. The T_m was calculated using the mean point of the Boltzmann sigmoidal non-linear regression [19,34,35].

2.8. Superoxide dismutase activity assays

The superoxide dismutase activity (SOD activity) of complexes **C1, C2, C3, C4** and **C5** was determined by measuring the inhibition of nitrotetrazolium blue chloride (NBT) photoreduction assays, according to a previously described procedure [11,36-42]. The reaction mixture consisted of 2.4 mL of a sodium phosphate buffer solution (pH = 7.8) containing 9.53 x 10^{-3} mol/L of methionine and 3.8 x 10^{-5} mol/L of NBT. Temperature was set to 25 ºC. A 50 µL aliquot of a dilute solution containing the complexes in DMF was added to the solutions, followed by addition of riboflavin (final concentration = 3.2 x 10^{-6} mol/L). All experiments were conducted in triplicate, included the blank samples (only solvent, no added complex). The solutions were illuminated with a fluorescent lamp at constant light intensity. NBT reduction was monitored spectrophotometrically at λ = 560 nm as a function of the illumination period (*t*). NBT reduction rate in the absence and in the presence of complexes were determined for a range of complex concentrations.

Inhibition percentage was calculated according to $\{(\Delta_{Abs}/t)_{without\ complex} - (\Delta_{Abs}/t)_{with\ complex}\} \times 100/(\Delta_{Abs}/t)_{without\ complex}$. The IC_{50} values represent the concentration of the SOD mimic that induces a 50% inhibition of NBT reduction. The catalytic rate constants (kinetic constants of McCord and Fridovich*)* were calculated as $k_{McCF} = k_{NBT}$ [NBT]/IC_{50}, where k_{NBT} (pH = 7.8) = 5.94 x 10^4 M^{-1} s^{-1} [43].

2.9. Catecholase activity

The catalytic activity of the copper(II) complexes was evaluated by the oxidation reaction using 3,5-di-tert-butylcatechol as substrate (3,5-DTBC). Kinetic experiments were performed in duplicate under substrate excess conditions by monitoring spectrophotometrically on a UV-vis spectrometer Varian Cary 50 Bio coupled to a thermostated bath, the change in absorbance that occurred at 400 nm (ε = 1.645 M^{-1} cm^{-1}) due to formation of 3,5-di-tert-butilquinone (3,5-DTBQ). The reactions were monitored from 2 to 5% of substrate conversion to product and the data were treated by the method of initial rates, which were obtained directly from the substrate concentration *versus* time.

Optical glass cuvettes were used (4 mL) and optical path of 1.0 cm, closed with a teflon cap, to which was added 50 µL of aqueous solution ($[T]_{final}$ = 3.33 x 10^{-2} mol/L) buffers: (MES pH = 4.0 to 6.5 and TRIS pH = 7.0 to 10.0), 1100-1380 µL of methanol saturated with oxygen and 50 µL of a solution of compound in DMSO ($[C]_{final}$= 2.67 x 10^{-5} mol/L). The reaction was started by adding 50 to 300 µL of a methanolic solution of the substrate ([S] = 5.88 x 10^{-4} to 7.06 x 10^{-3} mol/L) and monitored for 10 minutes. In all experiments, the final volume of the reaction mixture in the cuvette was 1.5 mL, respectively.

Corrections spontaneous oxidation of the substrate 3,5-DTBC were performed under identical conditions without the addition of the complex. The initial rates were obtained from the slope of the absorbance *versus* time curve during the first minutes of the reaction by the method of initial rates. The formation of hydrogen peroxide in the oxidation reactions of 3,5-DTBC catalyzed by complexes **C1** to **C5** was detected by a modification of the iodometric method [44].

A reaction mixture was prepared similar to kinetic experiments: complex concentration $[C]_{Final}$ = 2.67 x 10^{-5} mol/L (pH = 6.5) and substrate concentration $[S]_{final}$ = 3.33 x 10^{-3} mol/L. After one hour of reaction, an equal volume of water was added and the quinone was extracted with dichloromethane. The aqueous layer was acidified with sulfuric acid ([Acid] = 5 x 10^{-3} mol/L) at pH ≅ 2, to stop the oxidation reaction, and 1.0 mL of aqueous solution of potassium iodide ([iodide] = 0.3 mol/L) were added.

In the presence of hydrogen peroxide is the following reaction:

$$\mathbf{H_2O_2 + 2H^+ + 2I^- \rightarrow I_2 + 2H_2O}$$

and iodide ion excess occurs the formation of triiodide ion:

$$\mathbf{I_{2(aq.)} + I^- \rightarrow I_3^-}$$

This reaction is usually slow, but in acid solution becomes virtually instantaneous. The formation of triiodide ion (I_3^-) can be monitored spectrophotometrically due to the emergence of a characteristic band at 353 nm (ε = 26.000 M^{-1} cm^{-1}).

*2.10. Ligand synthesis – General procedure (**Scheme 1**)*

In a round bottom flask, pyridoxal hydrochloride (0.201 g; 1.0 mmol) was added to methanol (15 mL) and the resulting suspension was subjected to magnetic stirring at room temperature until complete dissolution of the pyridoxal molecule. Then, the corresponding aniline (0.120 g of 2-fluoroaniline; 0.130 g of 2-chloroaniline, 0.170 g of 2-bromoaniline or 0.220 g of 2-iodoaniline; 1.0 mmol for each) dissolved in methanol (5 mL) was added. The resulting mixture was kept under magnetic stirring at reflux temperature for 2.0 h. After this period, the flask contents were cooled to room temperature and the solvent evaporated. The resulting solid was washed with small portions of ice water and diethyl ether and dried in a desiccator with $CaCl_2$. For the synthesis of the ligand containing aniline, the same conditions were used, but without potassium hydroxide (0.093 g of aniline was added to 15 mL of methanol and 1 mmol of pyridoxal hydrochloride; 0.201 g).

Insert Scheme1 about here

5-(hydroxymethyl)-2-methyl-4-(phenylimino)methyl)pyridin-3-ol (L1): Properties - light yellow crystals, yield 73%. Melting point: 223 °C. Anal.Calc. for $[C_{14}H_{14}N_2O_2]HCl$: C, 60.38; H, 5.43; N, 10.03. Found: C, 60.33; H, 5.42; N, 10.05%. IR (KBr pellets, cm^{-1}): 3218 [w, ν(O-H)]; 1605 [m, ν(C=N)]; 1375 [m, ν(C–N)], 1165 [s, $\nu(C\text{-}O)_{phenol}$], 1060 [s, $\nu(C\text{-}O)_{alcohols}$] and 655 [s, $\nu(O\text{-}H)_{alcohols}$] (w = weak; m = medium; s = strong). ^1H NMR (ppm, $CDCl_3$): δ 2.5 (s, 3H, CH_3); 4.84 (s, 2H, CH_2); 7.32-7.46 (m, 5H, Ar); 7.87 (s, 1H, Py) and 9.18 (s, 1H, CH_{imine}).

4-(2-fluorophenylimino)methyl)-5-(hydroxymethyl)-2-methylpyridin-3-ol (L2): Properties - yellow crystals, yield 71%. Melting point: 206 °C. Anal.Calc. for [$C_{14}H_{14}FN_2O_2$] C, 56.60; H, 4.75; N, 9.45. Found: C, 56.67; H, 4.76; N, 9.44%. IR (KBr pellets, cm^{-1}): 3124 [w, ν(O-H)]; 1612 [m, ν(C=N)]; 1388 [m, ν(C–N)], 1296 [s, $\nu(C\text{-}O)_{phenol}$]; 1090 [m, ν(C-F)]; 1026 [s, $\nu(C\text{-}O)_{alcohols}$] and 630 [s, $\nu(O\text{-}H)_{alcohols}$] (w = weak; m = medium; s = strong). ^{1}H NMR (ppm, DMSO-d_6): δ 2.45 (s, 3H, CH_3); 4.82 (s, 2H, CH_2); 7.04-7.68 (m, 4H, Ar); 8.03 (s, 1H, Py) and 9.30 (s, 1H, CH_{imine}).

4-(2-chlorophenylimino)methyl)-5-(hydroxymethyl)-2-methylpyridin-3-ol (L3): Properties - orange crystals, yield 83%. Melting point: 202 °C. Anal.Calc. for [$C_{14}H_{13}ClN_2O_2$] C, 53.70; H, 4.49; N, 8.89. Found: C, 53.69; H, 4.51; N, 8.94%. IR (KBr pellets, cm^{-1}): 3113 [w, ν(O-H)]; 1614 [m, ν(C=N)]; 1387 [m, ν(C–N)], 1263 [s, $\nu(C\text{-}O)_{phenol}$], 1026 [s, $\nu(C\text{-}O)_{alcohols}$], 855 [m, ν(C-Cl)] and 625 [s, $\nu(O\text{-}H)_{alcohols}$] (w = weak; m = medium; s = strong). ^{1}H NMR (ppm, DMSO-d_6): δ 2.46 (s, 3H, CH_3); 4.81 (s, 2H, CH_2); 7.41-7.69 (m, 4H, Ar); 8.03 (s, 1H, Py) and 9.25 (s, 1H, CH_{imine}).

4-(2-bromophenylimino)methyl)-5-(hydroxymethyl)-2-methylpyridin-3-ol (L4): Properties - orange crystals, yield 85%. Melting point: 207 °C. Anal.Calc. for [$C_{14}H_{13}BrN_2O_2$] C, 47.02; H, 3.95; N, 7.83. Found: C, 46.93; H, 3.90; N, 7.79%. IR (KBr pellets, cm^{-1}): 3209 [w, ν(O-H)]; 1627 [m, ν(C=N)]; 1387 [m, ν(C–N)], 1257 [s, $\nu(C\text{-}O)_{phenol}$], 1033 [s, $\nu(C\text{-}O)_{alcohols}$], 694 [m, $\nu(C\text{-}Br)_{alcohols}$] and 620 [s, $\nu(O\text{-}H)_{alcohols}$] (w = weak; m = medium; s = strong). ^{1}H NMR (ppm, DMSO-d_6): δ 2.46 (s, 3H, CH_3); 4.80 (s, 2H, CH_2); 7.32-7.81 (m, 4H, Ar); 8.03 (s, 1H, Py) and 9.21 (s, 1H, CH_{imine}).

4-(2-iodophenylimino)methyl)-5-(hydroxymethyl)-2-methylpyridin-3-ol (L5): Properties - orange crystals, yield 81%. Melting point: 214 °C. Anal.Calc. for [$C_{14}H_{13}IN_2O_2$] C, 41.56; H, 3.49; N, 6.92. Found: C, 41.50; H, 3.48; N, 6.99%. IR (KBr pellets, cm^{-1}): 3070 [w, ν(O-H)]; 1604 [m, ν(C=N)]; 1381 [s, ν(C–N)], 1265 [s, $\nu(C\text{-}O)_{phenol}$], 1026 [s, $\nu(C\text{-}O)_{alcohols}$], 615 [s, $\nu(O\text{-}H)_{alcohols}$] and 525 [m, $\nu(C\text{-}I)_{alcohols}$] (w = weak; m = medium; s = strong). ^{1}H NMR (ppm, DMSO-d_6): δ 2.46 (s, 3H, CH_3); 4.79 (s, 2H, CH_2); 7.14-8.00 (m, 4H, Ar); 8.03 (s, 1H, Py) and 9.12 (s, 1H, CH_{imine}).

*2.12. Copper(II) complexes synthesis – General procedure (**Scheme 2**)*

The synthesis of the complex **C1** was carried out *in situ*. Pyridoxal hydrochloride (0.203 g; 0.1 mmol), $CuCl_2.2H_2O$ (0.085 g; 0.05 mmol) and aniline (0.093 g; 0.1 mmol) were dissolved in methanol (10 mL). The solution was heated in an oil-bath at 50 ºC and stirred for 1 h. After 2 days, green crystals were obtained by slow evaporation of the solvent.

In a round bottom flask, the corresponding ligand (**L2**, **L3**, **L4** and **L5;** 0.1 mmol for each) was added to methanol (10 mL) and the resulting mixture was subjected to magnetic stirring until complete dissolution of the ligand, followed by addition of triethylamine (30 µL). In the next step, copper(II) perchlorate (0.187 g; 0.05 mmol) dissolved in methanol (5 mL) was added and the resulting solution was subjected to magnetic stirring at 60 °C for 1.5 h. After this period, the solution was cooled to room temperature and slow evaporation of the solvent resulted in crystals of complexes **C2-C5**.

Insert Scheme 2 about here

Complex C1: Red/green crystals. Yield: 70% Melting point: 212 °C (dec.). Anal.Calc: $C_{28}H_{32}N_4O_6Cl_2Cu$ (650,98 g.mol^{-1}): C, 51.38; H, 4.99; N, 8.52. Found: C, 51.34, H, 4.92; N, 8.55%. IR (KBr pellets, cm^{-1}): 3526 [m, $\nu(O–H)_{alcohols}$]; 1599 [s, $\nu(C=N)$]; 1415 [m, $\nu(C–O)_{phenol.}$]; 1312 [m, $\nu(O–H)_{alcohol}$] and 1012 [s, $\nu(C–O)_{alcohols}$].

Complex C2: Red crystals. Yield: 56% Melting point: 253-254 °C (dec.). Anal.Calc: $C_{28}H_{24}F_2N_4O_4Cu$ (582,06 g mol^{-1}): C, 57.80; H, 4.19; N, 9.62. Found: C, 57.78, H, 4.16; N, 9.63%. IR (KBr pellets, cm^{-1}): 3353 [m, $\nu(O–H)_{alcohols}$]; 1605 [s, $\nu(C=N)$]; 1421 [m, $\nu(C–N)$]; 1187 [m, $\nu(C–O)_{phenol}$]; 1044 [m, $\nu(C\text{-}F)$] and 1021 [s, $\nu(C–O)_{alcohols}$].

Complex C3: Red crystals. Yield: 90% Melting point: 208-209 °C (dec.). Anal.Calc: $C_{28}H_{24}Cl_2N_4O_4Cu$ (614,96 g mol^{-1}) C, 54.71; H, 3.91; N, 9.12. Found: C, 54.69, H, 3.93; N, 9.11%. IR (KBr pellets, cm^{-1}): 3153 [m, $\nu(O–H)_{alcohols}$]; 1603 [s, $\nu(C=N)$]; 1419 [m, $\nu(C–N)$.]; 1187 [m, $\nu(C–O)$phenol]; 1026 [s, $\nu(C–O)_{alcohols}$] and 767 [m, $\nu(C\text{-}Cl)$].

Complex C4: Red crystals. Yield: 96% Melting point: 255-256 °C (dec.). Anal.Calc: $C_{28}H_{24}Br_2N_4O_4Cu$ (703,86 g mol^{-1}) C, 47.80; H, 3.46; N, 7.99. Found: C, 47.78, H, 3.44; N, 7.96%. IR (KBr pellets, cm^{-1}): 2916 [m, $\nu(O–H)_{alcohols}$]; 1606 [s, $\nu(C=N)$]; 1420 [m, $\nu(C–N)$.]; 1187 [m, $\nu(C–O)_{phenol}$]; 1023 [s, $\nu(C–O)_{alcohols}$] and 735 [m, $\nu(C\text{-}F)$].

Complex C5: Red crystals. Yield: 93% Melting point: 255-256 ºC (dec.). Anal.Calc: $C_{28}H_{24}I_2N_4O_4Cu$ (797,86 g mol^{-1}). C, 42.04; H, 3.06; N, 6.97. Found: C, 42.15, H, 3.03; N, 7.02%. IR (KBr pellets, cm^{-1}): 3153 [m, $\nu(O–H)_{alcohols}$]; 1593 [s, $\nu(C=N)$]; 1422 [m, $\nu(C–N)$.]; 1193 [m, $\nu(C–O)_{phenol}$] and 563 [m, $\nu(C–I)$].

Insert Table 1 about here

3. RESULTS AND DISCUSSIONS

*3.1. Crystal structures of **C1**, **C2** and **C5***

In the molecular structure of complex **C1** (**Figure 1**), the copper(II) cation is bonded to two phenolic oxygen atoms, as well as to the two nitrogen atoms present in the imine function, thus giving a total of four bonds around the metallic center, with square planar coordination geometry. This is shown by the angles formed between the O(1)-Cu-O(1)# and N(2)-Cu-N(2)# Å; O(1)-Cu-N(2) Å atoms, which are respectively, 180(10)º and 89.53(7)º. These values are consistent with the literature [45]. The complex **C1** is similar to that described by Marinovich et al. [46]. Symmetry operations used to generate equivalent atoms: (#) $-x + 2$, y, $z + 2$.

The length of the bond involving the copper atom and the phenolic oxygen atoms of the ligand is 1.9134(15) Å, for Cu-O1. The Cu-N2 imine bond presented a distance of 2.0062(18) Å. As expected, these values are within the range of Cu-O and Cu-N bond

lengths reported in the literature ($Cu–O_{(phenol)}$ 1.87-1.88 Å and $Cu–N_{(imine)}$ 1.99 Å) [47,48]. Other relevant bond lengths and angles for the structural analysis of **C1** are shown in **Table S1** (see in the *supplementary information section*).

Insert Figure 1 about here

In the C2 complex, the coordination of the ligand (L2) is carried out through the iminic nitrogens, as well as from the phenolic oxygens of the two pyridoxal molecules (**Figure 2**). These bond distances are in accordance with literature values [49,50,51]. Other relevant bond lengths and angles for the structural analysis of **C2** are shown in **Table S1** (see in the *supplementary information section*).

Apparently, the fluorine atom does not produce a change in the metal-halogen interaction thus, a second molecule of the ligand is coordinated to the metal center generating the expected geometry.

Insert Figure 2 about here

Figure 1S (*supplementary information section*) allows the visualization of intermolecular O2#-H2#···N1 secondary interactions in the *bc* plane, and angles and distances confirm that these intermolecular bonds support the growth of a supramolecular assembly

of complex **C2** along the crystallographic *b* axis [4,52]. The comparison of hydrogen secondary bonds for compound **C2** is shown in **Table S2** (*supplementary information section*).

In addition to these intermolecular interactions, it is also noteworthy that along the *a* axis there is an expressive number of further trifurcated hydrogen bonding, as shown in **Figure 2S** (*supplementary information section*) [53-58]. These secondary bonds are of an electrostatic nature, but sometimes their nature can undergo variations. According to Desiraju and Steiner [57], for supramolecular organizations the directionality of the connection depends on the donor and the receiver.

In the case of complex **C5** (**Figure 3**), the ligand is also in bidentate mode, with the two phenolate oxygens and two iminic nitrogens in the equatorial positions. The bond distance values from the metal center to the imine nitrogen and the oxygen atoms of phenolate are in accordance with the literature [59]. The most relevant values for the bond lengths and angles of complex **C5** and a comparison to **C1** and **C2** complexes are listed in **Table S2** (see in the *supplementary information section*).

Insert Figure 3 about here

Although the secondary bonds of the iodine atom are below the sums of the Van der Waals rays (3.38 Å) [60], there is no evidence of the existence of bonds/interactions between Cu···I (**Figure 3S** in the *supplementary information section*). However, considering the secondary bonds of iodine and oxygen O2, the following packaging arrangement occurs: the bonding distance of the I···O2 is 2.979(1) Å and the angle is 170.53(2)°, these values being compatible with strong iodine···oxygen interactions [61].

*3.2. UV-vis analysis of copper complexes **C1-C5***

In general, for the free ligands **L1-L5** two bands were observed in the UV-vis spectra, which can be assigned to the π→π* intraligand transition at 298 nm (imine moiety) and the *n*→π* transition in the 345-349 nm range.

The electronic spectra of the mononuclear copper(II)-complexes **C1-C5**, measured in DMF solutions, reveal two strong absorption bands (**Table 3S** in the *supplementary information section*) (see **Figure 4S** in the *supplementary information section*) in the 290-500 nm range. While the band observed at 298 nm, can be assigned to the π→π* intraligand transition, the band in the 400-410 nm range is best described as being the result of a ligand-to-metal charge-transfer (LMCT) transition from pyridoxal to the Cu(II). In any case, *d-d* transitions were not observed in the 500-800 nm electronic spectra range under these experimental conditions due to the low solubility and absorption of these transitions. However, such transitions were clearly observed when solid state diffuse reflectance spectra of the complexes **C1-C5** were obtained (**Table 3S** in the *supplementary information section*).

*3.3. Electrochemical properties of copper(II) complexes **C1-C5***

Electrochemical analysis of the free ligands **L1-L5** was carried out through cyclic voltammetry in dry DMF solution and cyclic voltammograms (CV's) revealed the presence of one irreversible process in the anodic region, with oxidation peaks at E_{pa} = -0.08 V

(R = H), E_{pa} = +0.17 V (R = F), E_{pa} = +0.10 V (R = Cl), E_{pa} = +0.14 V (R = Br) and E_{pa} = +0.11 V (R= I), respectively, which can be attributed to ligand oxidation. In general, at the cathodic region (0.0 to -1.60 V), the *ortho*-substituted halogenated ligands presented a reduction peak in the -1.40 to -1.60 V potential range, which we tentatively attribute to the reduction of the imine group.

In the case of the copper(II) complexes, the cyclic voltammograms of **C1-C5** are presented in **Figure 4**. The CV´s of **C1-C5** in dry DMF solution display quasi-reversible redox responses in the -1.50 to -1.75 V potential range, which can be attributed to the one-electron Cu^{II}/Cu^{I} redox pair. These redox potentials lie in the range found for mononuclear Cu(II) complexes containing SALEN-type Schiff base ligands [62]. From the $E_{1/2}$ values listed in **Table 2**, it seems that the *ortho*-substituted haloanilines only slightly affect the N-donor capacity of the imine nitrogen coordinated to the copper(II) center. During the anodic potential scan, all the complexes show two irreversible oxidative responses in the -0.28 to +0.11 V range, which are most probably related to the sequential oxidation of the ligand molecules when coordinated to the Cu(II) center (**Figure 4**). The oxidation observed for the ligands **L1-L5** in the -0.08 – 0.17 V range and the presence of two oxidation processes for **C1-C5** strongly corroborates this assignment. In fact, the oxidation of the second ligand bound to Cu^{II} is expected to occur at a higher potential due to the loss of electronic density of the whole molecule when the first ligand becomes oxidized. All the potentials were referenced to the ferrocene/ferrocenium redox pair and potential values are listed in **Table 2.**

Insert Figure 4 about here

Insert Table 2 about here

3.4. DNA cleavage assays

All complexes were able to cleave DNA in a concentration-dependent mode, i.e. as the complex concentration in the reaction medium rises the DNA cleavage capacity also increases.

In this study, complex **C2** (R = F) presented the lowest cleavage capacity. When the DNA sample was treated with 10 μM of this Cu(II) complex, a single cleavage in the supercoiled DNA was observed generating a ~15% of FII (**Figure 5B**). The progressive raise in complex **C2** concentration raised the DNA cleavage reaching ~40% of FII with 250 μM of complex. The complexes with chlorine (complex **C3**) and bromine halogen (complex **C4**) presented a cleavage potential similar to the unsubstituted complex **C1** (**Figure 5A**, **4C** and **5D**). The DNA treated with 250 μM of these complexes presents a ~60% of FII. In comparison to these complexes, the one containing iodine (complex **C5**) demonstrated the higher activity, since at 250 μM concentration; ~80% of the DNA was present as FII (**Figure 5E**). At the concentration range of 100-250 μM it could be seen the formation of linear DNA (FIII) with ~10% and ~20% respectively, which indicates a double strand rupture of the DNA helix structure, being the last concentration all treated plasmid DNA was cleaved with ~80% of FII and ~20% of FIII. Although the reactivity order may be better clarified by kinetic tests, currently it can be suggested that: **C2** << **C4** ≈ **C3** << **C5**.

These results may indicate that there is a relationship between electronegativity and atomic radius of each halogen and the cleavage DNA potential, being the fluorine, having the highest electronegativity and smallest atomic radius, the one with lower cleavage potential. The iodine, having the lowest electronegativity and larger atomic radius, presented higher cleavage potential.

Insert Figure 5 about here

3.4.1. DNA groove binders: effect on cleavage

It was aimed to determine if the interaction between complex and DNA occurred due to dependency for minor or major DNA grooves. Tests were realized using minor and major groove blockers, respectively netropsin and methyl green. The results are presented in **Figure 6**.

Complex **C1** (control) and the copper(II) complexes **C3** and **C4** have shown a clear inhibition in the presence of the minor groove binder, netropsin, resulting in ~25% inhibition for complex **C1**, ~57% for the complex **C4**, and ~39% for the complex **C3**, respectively. This suggests that such Cu(II) complexes access the DNA by a minor groove interaction (**Figure 6**). The *ortho*-I-substituted complex **C5** has not shown an alteration of DNA cleavage in the presence of both groove binders. The *ortho*-F-substituted complex **C2** has not presented a cleavage alteration in the presence of the minor groove binder netropsin, however, in the presence of a major groove blocker, methyl green, the cleavage potential increased in ~40% (**Figure 6**). This may be explained by the methyl green interacting with the DNA and facilitating the access of the complex to the structure, raising the cleavage potential, effect that is already known and described for others groove binders such as distamicyn [62].

Insert Figure 6 about here

3.4.2. ROS scavengers effect on cleavage

Since the description by Sigman and co-workers [63] of the metallic complexes capacity to cleave DNA generating reactive oxygen species, studies were conducted to investigate the potential cleavage mechanism for each metal new complex described. Reactive oxygen species (ROS) can be formed by the reduction of molecular oxygen, which can result in damage to the DNA by oxidative cleavage [64]. Thus the DNA cleavage potential in the presence of two ROS scavenger species were tested, being potassium iodine (KI) as scavenger of superoxide radical and sodium azide (NaN_3) as singlet oxygen inhibitor.

Results presented in **Figure 7** indicate that the cleavage mechanism of such copper(II) complexes should not be dependent of this ROS, since no cleavage inhibition is seen in the presence of the scavengers, excepting in the case of the complex containing bromine atom (complex **C4**). This complex presented a slight inhibition in the presence of the scavenger species, but still not enough to confirm dependency [65]. The present results also indicate that the complexes cleave DNA through a hydrolytic mechanism, although, it was reported that other complexes are able to oxidize directly the DNA molecule (the DNA cleavage potential of the complexes was not affected in anaerobiosis (**Figure 5S** (*supplementary information section*), thus the reaction seems to be independent of oxygen), without the generation of a reactive species [66-69].

Insert Figure 7 about here

3.4.3. DNA cleavage kinetics

The kinetic profile of DNA cleavage promoted by the copper(II) complexes was determined by disappearance of the supercoiled plasmid DNA form (FI) as a function of time (**Figure 8**). Considering the data as a *pseudo*-first-order reaction kinetic

[70] where there is an excess of catalyzer relative to substrate, the cleavage DNA observed constant (k_{obs}) and half-life time ($t_{1/2}$) are presented in the inset of **Figure 8**.

Kinetic tests were performed at a single concentration, being 250 μM for all complexes, except for the complex **C5** (R = I), for which were used a lower concentration (50 μM), since it is the most active. The test indicates significant difference among the observed constants from different derivatives, the complex with fluorine atom (complex **C2**) presenting a lower k_{obs} and consequently higher half-life time for the cleavage of the DNA form, corroborating with the results found at the concentration dependence test (**Figure 8**). The complexes containing chlorine and bromine atoms (complexes **C3** and **C4**) presents difference in the k_{obs} constants, diverging from the concentration tests, which showed a similar cleavage potential. At the kinetic test, the complex **C3** presents a higher k_{obs} in comparison to Br-substituted complex **C4** (**Figure 8**). The complex containing iodine atom in the *ortho* position (complex **C5**), even in at 5 times lower concentration, presented a lower half-life time relative to complex **C3** (R = Cl), which presented the higher k_{obs} at the 250 μM concentration (**Figure 8A-E**).

Thus, once more the complex **C5** containing the iodine halogen atom is more active, and considering the data obtained by the kinetic assay it is possible to express the following cleavage potential order: **C2**<< **C4** << **C3** <<**C5**.

Insert Figure 8 about here

3.5. Thermal denaturation

The thermal denaturation assays were conducted with the complex that contains iodine atom (complex **C5**), the most active, and also with a control complex without halogen (Cu-aniline – complex **C1**), and another control only with DNA and solvent (DMSO). The experiment was performed with the concentration of 5 μM complex.

The found DNA thermal denaturation temperature (T_m) without complexes was 58,6ºC, while in the presence of complex **C5** the T_m raised to 60.0ºC. The increase in the T_m was not sufficient to confirm that the complex increased the DNA denaturing temperature as result of interaction between them (**Figure S6** in the *supplementary information section*).

3.6. Evaluation of superoxide dismutase mimetic activity (SOD)

We have evaluated the mimetic activity of superoxide dismutase of ligands and coordination compounds by analyzing inhibition of the reaction between the superoxide ion and NBT and consequent formazan production. Thus, compounds that have antioxidant activity are able to react more easily with superoxide radicals.

The reaction was monitored spectrophotometrically at 560 nm and the mean absorbance of triplicate values was subtracted from the absorbance values obtained for the sample considered control. Thus, the result expressed as superoxide ion production was inhibited at each concentration of the antioxidant. This value is then expressed as a percentage of inhibition of photoreduction reaction of NBT. The straight line equation was used to quantify the IC_{50} value, the concentration which inhibits 50% of the reaction, in order to relate the various concentrations of the compound tested with their respective percentages of inhibition of NBT photoreduction.

The results demonstrate that some coordination compounds exhibited potential for inhibition of the superoxide ion while the ligands did not demonstrate such a function.

When the halogen of the *ortho*-substituted was evaluated, it was found that the C2 complex containing the 2-fluoroaniline ligand showed unsatisfactory disproportionation of superoxide ion. This fact can be explained by the high electronegativity of the fluorine atoms that lead to a greater polarization of charges in the complex molecule, forming a negative pole that repels the superoxide radical, making it difficult to approach to the metal center, which consequently promote the reaction between the superoxide and NBT molecules. On the other hand, the complex containing iodine exhibits better IC_{50} values compared to the other complexes, this can be explained (associated) to the lower value of the reduction potential of Cu (II)-Cu(I) species (**Table 2**), thus, the dismutation of the superoxide ion promoted by copper occurs easily.

Values of the catalytic rate constants for superoxide disproportionation shown in **table 3** clearly indicate that these complexes can be used as superoxide scavengers. Comparison of kMcCF of copper complexes and bibliographic references with similar complexes, with C5 being the most suitable for reacting with superoxide.

Insert Table 3 about here

3.6. Catecholase activity assay

Several studies in the literature report on the catalytic activity of Cu (II) mononuclear complexes tested on the oxidation of the substrate model 3,5-di-tert-butylcatechol (3,5-DTBC). This substrate is widely used an oxidative model due to its low redox potential

that facilitates oxidation in quinone (3,5-DTBQ), furthermore, the presence of bulky substituents promotes secondary reactions of oxidation, such as ring opening [75 76,77].

The data obtained from kinetic studies of oxidation of 3,5-DTBC promoted by complexes of **C1** to **C5**, were treated by monitoring the appearance of the intense absorption band at 400 nm region, as a result of the formation of the corresponding quinone (3,5-DTBQ; ε = 1.900 L/mol.cm). A kinetic study carried out for C1-C5, under anaerobic conditions, shows that only one equivalent of the substrate is oxidized to 3,5-DTBQ (stoichiometry substrate:complex 1:1). Such results suggest that two mononuclear Cu(II) centers of the catalyst should be reduced to Cu(I) in a simultaneous two-electron transfer process. The interaction of the 3,5- DTBC substrate with two mononuclear **C1-C5** units is assumed to generate the Michaelis intermediate. When oxygen (O_2) was bubbled into the solution immediately the catalytic activity is regenerated indicating that the catalyst is still active and must participate directly in the catalytic cycle acting as a thermodynamic driving force by reoxidizing any Cu(I) species back to the active Cu(II) complex [77,44,78].

In order to determine the influence of pH on the catalytic activity of **C1-C5**, reactions were carried out in the pH range 4.0 to 10.0. The dependence of the reaction rate (v_0) on pH for all complexes is given in **Figure 9(9A)**. Interestingly, for all the complexes, bell shape profiles (but not well defined) were observed and a pH optimum of 6.4 was determined. In addition, a kinetic pK_a of about 5.5 can be extracted for **C1** to **C5**. Drop in activity at pH ≥ 6.5 most probably occurs due to the presence of Cu^{II} coordinated OH^- groups which reduces the association of the substrate 3,5-DTBC to the catalyst. It is reasonable to assume that in solution, under the present kinetic experimental conditions a H_2O/OH^- ligand occupies the fifth Cu^{II} coordination site [77].

Insert Figure 9 about here

After defining the ideal pH for the oxidation of 3,5-DTBC by complexes **C1**-**C5**, dependence studies of the reaction rate on the substrate concentration were performed. For comparison, all curves were obtained at pH = 6.4. The graph of initial rates of the reaction (V_o) *versus* concentration of 3,5-DTBC show saturation profiles (**Figure 9B**), which suggests the formation of an intermediate substrate/complex and thus can be treated by the Michaelis-Menten model developed for enzyme kinetics. Kinetic parameters were obtained from nonlinear fits of the curves and the results are presented in **Table 4.**

Insert Table 4 about here

In general, the kinetic parameters found for complexes **C1** to **C5** are comparable to those previously reported for mono- di- and poly-nuclear copper(II) complexes [17,18,19,44]. From the data shown in **Table 4** it's possible to observe that the catalytic activity (k_{cat}) of these complexes is of the same magnitude but with complex **C5** being slightly more active. In fact, these experimental results are in full agreement with the cyclic voltammetric data, which clearly show that $E_{1/2}$ of **C5** is anodic shifted by ~150 mV when compared to **C1**-**C4**, due to the iodine substituent at the aniline ring. On the other hand, complex **C1** shows the lower K_M value within the series of complexes, a result which is most probably related to some steric effect of the halogen substituents in **C4**-**C5**. At this stage it is important to emphasize that under the kinetic experimental conditions, it is assumed that a dimer is most probably the catalytically active species in the oxidation of 3,5-DTBC. Indeed, several factors need to be considering in assessing the difference in catalytic activity of these complexes. For the complexes shown in the present work, it seems that electrochemical properties and steric match play the major role in reactivity of complexes **C1**-**C5**.

Finally, the peroxide detection was performed according to the iodometric method proposed by Meyer and co-workers [79], which detected the presence of H_2O_2 accumulation compared with the experiment without the presence of the catalyst. This implies that the mechanism of catalysis performed by complexes **C1** to **C5**, is different from that proposed for the native enzyme [80] and is likely a 1:1 stoichiometric process 3,5-DTBC + O_2 → 3,5-DTBQ + H_2O_2 without the formation of water in the catalytic cycle.

6. FINAL REMARKS

Schiff base-type ligands derived from pyridoxal and halogen-substituted anilines showed great potential to coordinate copper(II) ions. The X-ray diffraction analysis revealed that the complexes presented square planar geometry with N_2O_2 donor atoms. The structures of **C2** and **C5** complexes present crystalline networks with hydrogen bonding and substantially distinct interactions, although they have the same spatial group and coordination environment.

All copper complexes showed antioxidant activity as mimetic for SOD, however, the best result was found with the complex containing *ortho* iodine which is the strongest oxidant within the series of complexes. On the other hand, the complex containing fluorine in the *ortho* position presented inexpressible IC_{50}% showing a clear trend related to electronic conditions generated by the substituents DNA and cathecolase.

Finally, cathecolase activity of the complexes in the oxidation of 3,5-di-tert-butylcatechol reveals that complex **C5**, containing the iodine substituent at the aniline ring and the highest $E_{1/2}$ value, also shows the highest catalytic activity. A similar trend was found for DNA cleavage, leading us to conclude that these complexes are able to directly oxidize the DNA molecule without the generation of ROS.

7. SUPPLEMENTARY DATA

CCDC 1544902, 1544903 and 1544904 contain the supplementary crystallographic data for this paper. These data can be obtained free of charge at http://www.ccdc.cam.ac.uk/conts/retriev-ing.html, or from the Cambridge Crystallographic Data Centre at 12 Union Road, Cambridge CB2 1EZ, UK; fax: (+44) 1223-336-033; or e-mail: deposit@ccdc.cam.ac.uk.

8. ACKNOWLEDGMENT

Brazilian Research Councils: CNPq – Edital Nº 14/2014 /Proc. Num. 443625/2014-0, 444780/2014-9 and Edital Nº 12/2016/ Proc. Num. 303011/2016-5. Edital Nº
007/2016 - PROBIC/FAPERGS/UFSM.

9. REFERENCES

[1] F. Xue, X. Xiao, H. Wang, Y. Shi, *Tetrahedron*. (2012) 6862.

[2] S. Scharif, D. Schagen, M.D. Toney, H.H. Limbach, *J. Am. Chem. Soc.* 129 (2007) 4440.

[3] D.F. Back, G.M. de Oliveira, L.A. Fontana, A. Neves, B.A. Iglesias, T.P. Camargo, P.T. Campos, J.P. Vargas, *Inorg. Chim. Acta.* 428 (2015) 163.

[4] J.D. Siqueira, A.C.O. Menegatti, H. Terenzi, M.B. Pereira, D. Roman, E. F. Rosso, P.C. Piquini, B.A. Iglesias, D.F. Back, *Polyhedron*. 130 (2017) 184.

[5] T. Mukherjee, J.C. Pessoa, A. Kumar, A.R. Sarkar, *Inorg. Chem*. 50 (2011) 4349.

[6] D.F. Back, G.M. de Oliveira, L.A. Fontana, B.F. Ramão, D. Roman, B. A. Iglesias, *J. Mol. Struct.*1100 (2015) 264.

[7] T. Rosu, E. Pahontu, M. Reka-Stefana, D.C. Ilies, R. Georgescu, S.Shova, A. Gulea, *Polyhedron,* 31 (2012) 352.

[8] M. Belicchi-Ferrari, F. Bisceglie, C. Casoli, S. Durot, I. Morgenstern-Badarau,G. Pelosi, E. Pilotti, S. Pinelli, P. Tarasconi, *J. Med. Chem*. 48, (2005) 1671.

[9] J.S. Casas, M.D. Couce, A. Sanchez, J. Sordo, E.M.V. Lopez. *J. Organomet. Chem.* 696 (2012) 4236.

[10] D. Pandiarajan, R. Ramesh, Y. Liu, R. Suresh, *Inorg. Chem. Commun.* 33 (2013) 33.

[11] S. Signorella, V. Daier, G. Ledesma, C. Palopoli, D.F. Back, E.S. Lang, C.R. Koppe, P. Ebani, M.B. Pereira, C. Giacomelli, P.C. Piquini, *Polyhedron.* 102 (2015) 176.

[12] F.C. Friedel, D. Lieb, I.I. Burmazović, *J. Inorg. Biochem.* 109 (2012) 26.

[13] H.Y.V. Ching, I. Kenkel, N. Delsuc, E. Mathieu, I.I. Burmazović, C. Policar, *J. Inorg. Biochem.* 160 (2016) 172.

[14] M.S. Islas, T. Rojo, L. Lezama, M.G. Merino, M.A. Cortes, M.R. Puyol, E.G. Ferrer, P.A.M. Williams, *J. Inorg. Biochem.* 123 (2013) 23.

[15] D.S. Sigman, A. Mazumder, D.M. Perrin, *Chem. Rev.* 93 (1993) 2295.

[16] V. Uma, M. Kanthimathi, T. Weyhermuller, B.U. Nair, *J. Inorg. Biochem.* 99 (2005) 2299.

[17] R.E.H.M.B. Osório, A. Neves, T.P. Camargo, S.L. Mireski, A.J. Bortoluzzi, E.E. Castellano, W. Haase, Z. Tomkowicz, *Inorg. Chim. Acta*, 435 (2015) 153.

[18] T.P. Camargo, R.A. Peralta, R. Moreira, E.E. Castellano, A.J. Bortoluzzi, A. Neves, *Inorg. Chem. Commun.* 37 (2013) 34.

[19] T. Bortolotto, P.P. Silva, A. Neves, E.C.P. Maia, H. Terenzi. *Inorg. Chem.* 50 (2011) 10519.

[20] R. Bushtit, Z. Trávníček, J. Vančo, *J. Inorg. Biochem.* 116 (2012) 163.

[21] K. Jitsukawa, M. Harata, H. Arii, H. Sakurai, H. Masuda, *Inorg. Chim. Acta,* 324 (2001) 108.

[22] R. Novotná, R. Herchel, Z. Trávníček, *Polyhedron*, 34 (2012) 56.

[23] S. Tabassum, S. Amir, F. Arjmand, C. Pettinari, F. Marchetti, N. Masciocchi, G. Lupidi, R. Pettinari, *Eur. J. Med. Chem.* 60, (2013) 216.

[24] R.R. Gagne, C.A. Koval, G.C. Lisensky, *Inorg. Chem*. 19 (1980) 2854.

[25] G.M. Sheldrick, *Acta Cryst. A* 6 (2008) 11.

[26] K. Brandenburg, *DIAMOND* 3.1ª. 1997–2005, Version 1.1ª. Crystal Impact GbR , Bonn, Germany.

[27] F.M. Ausubel, R. Brent, R. E. Kingston, D. D. Moore, J. G. Seidman, J. A. Smith, K. Struhl. *Short Protocols in Molecular Biology: A Compendium of Methods from Current Protocols in Molecular Biology*. 4ª Ed. New York: Wiley, 1999.

[28] M.C.B. Oliveira, D. Mazera, M. Scarpellini, P.C. Severino, A. Neves, H. Terenzi, *Inorg. Chem*. 48 (2009) 2711.

[29] Y. Jin, M.A. Lewis, N.H. Gokhale, E.C. Long, J.A. Cowan. *J. Am. Chem. Soc.* 129 (2007) 8353.

[30] K. Schlacher, P. Pham, M.M. Cox, M.F. Goodman, *Chem. Rev.* 106(2) (2006) 406.

[31] M.W. Van Dyke, R.P. Hertzberg, P.B. Dervan, *Proc. Natl. Acad. Sci.* USA. 79 (1982) 5470.

[32] S.K Kim, B. Nordén, *FEBS Lett.* 315 (1993) 61.

[33] D.L. Nelson, M.M. Cox, A.L. Lehninger, *Principles of Biochemistry*. 5ª, São Paulo: Sarvier. 2011.

[34] M.S. Arias, M.G. Álvarez, M.J. Fernández, A. Lorente, G. Alzuet, J. Borrás, *J. Inorg. Biochem*. 103 (2009) 1067.

[35] J.L. G. Giménez, G. Alzuet, M.G. Alvarez, M.L. González, A. Castiñeiras. J.Borrás, *J. Inorg. Biochem*. 103, (2009) 243.

[36] E. Üstün, M. Ç. Ayvaz, M. S. Çelebi, G. Aşcı, S. Demir, I. Özdemir, *Inorg. Chim. Acta*. 450 (2016) 182.

[37] C. Beauchamp, I. Fridovich, *Anal. Biochem*. 44 (1971) 276.

[38] B. Verdejo, S. Blasco, E.G. España, F. Lloret, P. Gaviña, C. Soriano, S. Tatay, H. R. Jiménez, A. Doménech, J. Latorre. *Dalton Trans*. 41 (2007) 4726.

[39] I. Szilágyi, I. Labádi, K. Hernadi, I. Pálinkó, I. Fekete, L. Korecz, A. Rockenbauer, T. Kiss, *New J. Chem.* 29 (2005) 740.

[40] O. Iranzo, *Bioorg. Chem*. 39 (2011) 73.

[41] P.R. Ebani, L. A. Fontana, P. T. Campos, E. F. Rosso, P. C. Piquini, B. A. Iglesias, D. F. Back, *J. Mol. Struct.* 1120 (2016) 163.

[42] C.M. Canabarro, J. Ceolin, J.D. Siqueira, B.A. Iglesias, G.M. de Oliveira, D.F. Back, P.T. Campos, *Z. Anorg. Allg. Chem*. 642, (2016) 1192.

[43] M.J. McCord, I. Fridovich, *J. Biol. Chem.* 244 (1969) 6049.

[44] A. Neves, I. M. Rossi, A.J. Bortoluzzi, B. Szpoganicz, C. Wiezbicki, E. Schwingel, *Inorg.Chem.* 41 (2002) 1788.

[45] J.L. van Wyk, S. Mapolie, A. Lennartson, M. Håkansson, S. Jagner, *Z. Naturforsch*, 62:b (2007) 331.

[46] A.F. Marinovich, R.S. O'Mahony, J.M. Waters, T.N.M. Waters, *Croat. Chem. Acta.* 72 (1999) 685.

[47] A. Takeuchi, H. Kuma, S. Yamada, *Synth. React. Inorg. Met. -Org. Chem.* 24 (1994) 171.

[48] B. Kamenar, A. Stefanovic, S. Antolic, *Z. Kristallogr*. 210 (1995) 730.

[49] V.T. Kasumov, I. Ucar, A. Bulut, *J. Fluorine Chem.* 131 (2010) 59.

[50] H. Unver, D.M. Zengin, T.N. Durlu, *J. Chem. Crystallogr*. 33 (2003)253.

[51] L.G. Wang, Y.F. Zheng, *Acta Cryst. E63* (2007) m390.

[52] M.B. Pereira, C.R. Kopp, L.A. Fontana, G.M. de Oliveira, D.F. Back, P.C. Piquini, M.A. Villetti, *New J. Chem.* 38 (2014) 3092.

[53] D.F. Back, G. Manzoni de Oliveira, M. Hörner, F. Broch, *Polyhedron*. 31 (2012) 558.

[54] L. Chęcińska, S.J. Grabowski, M. Małecka, *J. Phys. Org. Chem*. 16 (2003) 213.

[55] L.S. Glass, B. Nguyen, K.D. Goodwin, C. Dardonville, W.D. Wilson, E.C. Long, M.M. Georgiadis, *Biochemistry*. 48 (2009) 5943.

[55] P. Sharma, M. Chawla, S. Sharma, A. Mitra, *RNA 16* (2010) 942.

[57] G.R. Desiraju, T. Steiner, *Structural Chemistry and Biology: The Weak Hydrogen Bond (International Union of Crystallography – Monographs on Crystallography)*, Oxford University Press, 2001.

[58] T. Steiner, *Angew. Chem. Int.* Ed., 41 (2002) 48.

[59] H. Ünver, *J. Mol. Struct*. 641 (2002) 35.

[60] J. B. Mann, *Atomic Structure Calculations II. Hartree-Fock wave functions and radial expectation values: hydrogen to lawrencium*, LA-3691, Los Alamos Scientific Laboratory, USA .1968.

[61] K.S. Shin, M. Brezgunova, O. Jeannin, T. Roisnel, F. Camerel, P.A. Senzier, M. Fourmigué. *Cryst. Growth Des*. 11 (2011) 5337.

[62] Y. Hiraku, S. Oikawa, S. Kawanishi, *Nucleic Acids Symposium Series*. 2 (2002) 95.

[63] D.S. Sigman, D.R.Graham, V. D'Aurora, A.M. Stern, *J. Biol. Chem*. 254 (1979) 12269.

[64] Q. Jiang, N. Xiao, P. Shi, Y. Zhu, Z. Guo, *Coord. Chem. Rev*. 251 (2007)1951 .

[65] F. Mancin, P. Scrimin, P. Tecilla, U. Tonellato, *Chem. Commun*.
2005, 2540.

[66] P.U. Maheswari, M. van der Ster, S. Smulders, S. Barends, G.P. van Wezel, C. Massera, S. Roy, H. den Dulk, P. Gamez, J. Reedijk, *Inorg. Chem.* 47 (2008) 3719.

[67] M.S. Melvin, K.E. Wooton, C.C. Rich, G.R. Saluta, G.L. Kucera, N. Lindquist, R.A. Manderville, *J. Inorg. Biochem*. 87 (2001) 129.

[68] P.P. Silva, W. Guerra, J.N. Silveira, A.M.C. Ferreira, T. Bortolotto, F.L. Fischer, H. Terenzi, A. Neves, E.C.P. Maia, *Inorg*. Chem. 50 (2011) 6414.

[69] J. Tan, B. Wang, L. Zhu, *J. Biol. Inorg. Chem*. 14 (2009) 727.

[70] J.A. Cowan, *Curr. Opin. Chem. Biol.* 5 (2001) 634.

[71] H.D. Bian, J. Wang, Y. Wei, J. Tang, F.P. Huang, D. Yao, Q. Yu, H. Liang, *Polyhedron*. 90 (2015) 147.

[72] S. Çay, M. Köse, F. Tümer, A. Gölcü, M. Tümer, *Spectrochim. Acta Part A: Molecular and Biomolecular Spectroscopy*. 151 (2015) 821.

[73] R. S. Joseyphus, C. Shiju, J. Joseph, C. J. Dhanaraj, D. Arish. *Spectrochim. Acta Part A: Molecular and Biomolecular Spectroscopy* 133 (2014) 149.

[74] E. M. Niecy, L. P. Nitha, R. Aswathy, B. Sindhukumari, K. Mohanan. *Med. Chem. Res*. 24 (2015) 63.

[75] M.K. Panda, M.M. Shaiki, R.J. Butcher, P. Ghosh, *Inorg. Chim. Acta*, 372 (2011) 145.

[76] R. Marion, N.M. Saleh, N.L. Poul, D. Floner, O. Lavastre, F. Geneste, *New J. Chem*. 36 (2012)1828.

[77] R.E.H.M.B. Osório, R.A. Peralta, A.J. Bortoluzzi, V.R. de Almeida, B. Szpoganicz, F.L. Fischer, H. Terenzi, A.S. Mangrich, K.M. Mantovani, D.E.C. Ferreira, W.R. Rocha, W. Haase, Z. Tomkowicz, A. dos Anjos, A. Neves, *Inorg. Chem*. 51 (2012) 1569.

[78] E.I. Solomon, D.E. Heppner, E.M. Johnston, J.W. Ginsbach, J. Cirera, M. Qayyum, M.T.K. Emmons, C.H. Kjaergaard, R.G. Hadt, L. Tian, *Chem. Rev.* 114 (2014) 3659.

[79] J. Ackermann, F. Meyer, E. Kaifer, H. Pritzkow, *Chem. Eur. J.* 8 (2002) 247.

[80] S.A.Z. Senior, L.L. Mans, H.D. Van Guilder, K.A. Kelly, M.P. Hendrich, T.E. Elgren, *Biochemistry*, 42 (2003) 4392.

Caption for schemes

Scheme 1. Synthesis of ligands through condensation reaction of pyridoxal with *ortho*-halogenated substituted anilines.

Scheme 2. Synthesis of copper(II) complexes **C1-C5**.

Scheme1

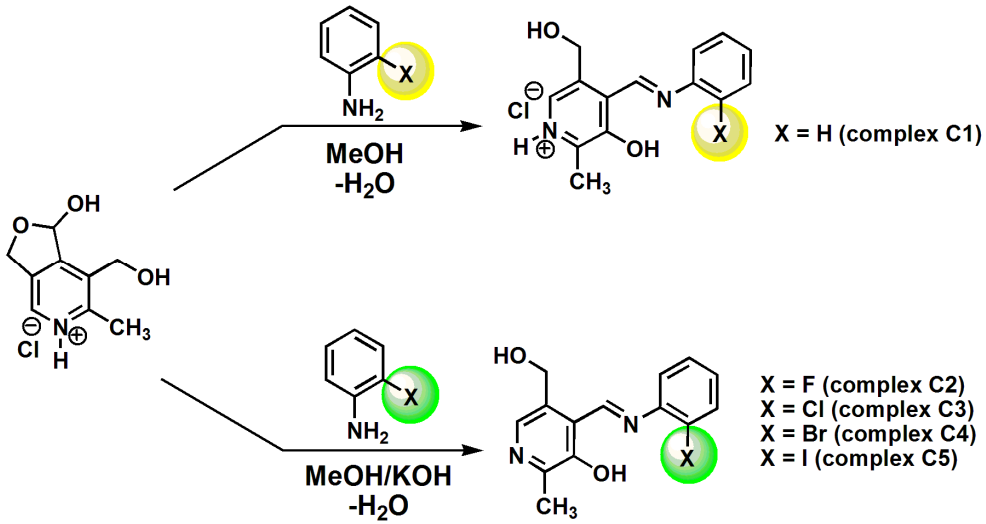

Scheme 2

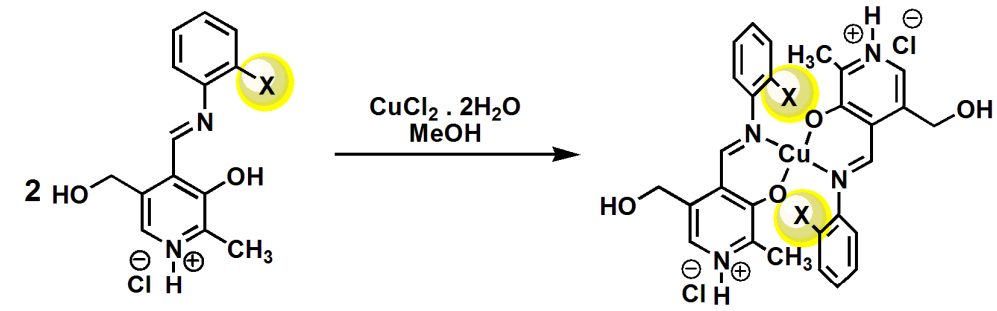

X = H (complex C1)

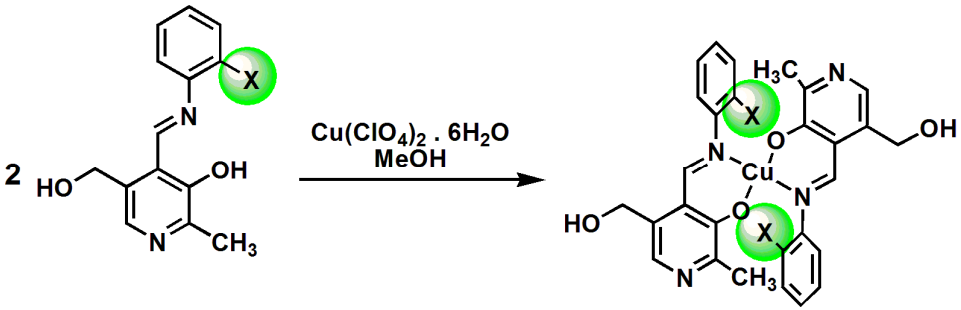

X = F (complex C2)
X = Cl (complex C3)
X = Br (complex C4)
X = I (complex C5)

Caption for tables

Table 1. Crystal data and structure refinement for **C1**, **C2** and **C5.**

Table 2. Redox potential values of free ligands **L1-L5** and copper(II)-complexes **1-5**, in DMF solutions scan rate at 100 mV/s.

Table 3. Superoxide dismutase mimetic activity data of copper complexes **C1**-**C5**.

Table 4. Kinetic parameters for the oxidation of 3,5-DTBC catalyzed by **C1**-**C5**.

Table 1

	C1	**C2**	**C5**
Empirical formula	$C_{28}H_{32}Cu_1Cl_2N_4O_6$	$C_{28}H_{24}CuF_2N_4O_4$	$C_{28}H_{24}CuI_2N_4O_4$
Formula weight	605.03	582.05	797.86
Crystal system, space group	triclinic, *P* -1	Monoclinic, $P2_1/c$	Monoclinic, $P2_1/c$
T / K	100K	100K	100K
Radiation, λ / Å	0.71073	0.71073	0.71073
Unit cell (Å) dimensions *a*, *b*, *c*	7.931 (4)	5.8822 (2)	7.7542 (3)
	9.709 (5)	20.7073 (5)	19.1151 (7)

	11.053 (9)	10.3709 (3)	10.5422 (5)
α, β, γ (°)	113.84 (5)	90	90
	96.65 (4)	102.226 (2)	111.277 (2)
	105.52 (5)	90	90
V (Å^3)	725.5 (8)	1234.57 (6)	1456.08(10)
Z, Calculated density (g.cm^{-3})	1, 1.499	2, 1.566	2, 1.820
Absorption coefficient (mm^{-1})	0.986	0,994	2.910
F (000)	339	598	774
Crystal size (mm)	0.38x 0.154 x 0.140	0.323x0.172x 0.134	0.41x0.40x0.32
Theta range for data collection	2.08 – 27.83	1.97 - 27.12	2.33 – 27.15
Index ranges	$-10 \leq h \leq 9$	$-7 \leq h \leq 7$	$-9 \leq h \leq 9$
	$-12 \leq k \leq 12$	$-26 \leq k \leq 26$	$-24 \leq k \leq 24$
	$-14 \leq l \leq 14$	$-13 \leq l \leq 13$	$-12 \leq l \leq 13$
Reflections collected / unique	19610 / 3442 [R(int) = 0.0338]	18730 / 2733 [R(int) = 0.0471]	18294 / 3221 [R(int) = 0.0239]
Completeness to theta max	99.7%	99.9 %	99.8%
Absorption correction	Multi-scan	Multi-scan	Numerical
Max. and min. transmission	0.9113 and 0.9003	0.9412 and 0.8533	0.4561and 0.3817
Refinement method	Full-matrix least-squares on F^2	Full-matrix least-squares on F^2	Full-matrix least-squares on F^2
Data / restraints / parameters	3453 / 0 / 187	2733 / 0 / 178	3221 / 0 / 178
Goodness-of-fit on F^2	1.062	1.092	1.079
Final R indices [I > 2σ(I)]	R1 = 0.0361, wR2 = 0.0876	1 = 0.0399, wR2 = 0.1177	R1 = 0.0366, wR2 = 0.0971
R indices	R1 = 0.0526, wR2 = 0.0947	R1 = 0.0611, wR2 = 0.1372	R1 = 0.0406, wR2 = 0.0990

Largest diff. peak and hole ($e.Å^{-3}$)	0.515 and -0.271	0.696 and -0.608	0.410 and -0.325

Table 2

	Oxidation			Reduction	
Ligands	E_{ox1}	E_{ox2}	E_{ox3}	E_{red1}	E_{red2}
L1	-0.08 V[a]	+0.25 V[a]	-----	-----	-1.51 V[b]
L2	+0.17 V[a]	-----	-----	-----	-1.40 V[b]
L3	+0.10 V[a]	-----	-----	-----	-1.41 V[b]
L4	+0.14 V[a]	-----	-----	-----	-1.42 V[b]
L5	+0.11 V[a]	-----	-----	-----	-1.45 V[b]
Complexes	E_{ox1}	E_{ox2}	E_{ox3}	E_{red1}	E_{red2}
C1	-0.28 V[a]	+0.02 V[a]	-----	-1.59 V[c]	-----
C2	-0.23 V[a]	+0.05 V[a]	-----	-1.59 V[c]	-----

C3	-0.20 V[a]	+0.08 V[a]	-----	-1.54 V[c]	-----
C4	-0.20 V[a]	+0.11 V[a]	-----	-1.52 V[c]	-----
C5	-0.09 V[a]	+0.03 V[a]	+0.21 V[a]	-1.39 V[c]	-----

[a]E_{pa} = anodic peak; [b]E_{pc} = cathodic peak;[c]$E_{1/2}$ = (E_{pa} + E_{pc}) / 2; scan rate at 100 mV/s.

Table 3

Compound	IC_{50} µM	Indicator/ $[\ ]_{Ind}$ (µM)	k_{McCF} ($M^{-1}s^{-1}$)x10^6
C1	1.01	NBT/ 38 µM	2.23
C2	48.30	NBT/ 38 µM	0.05
C3	1.43	NBT/ 38 µM	1.59
C4	1.09	NBT/ 38 µM	2.07
C5	0.40	NBT/ 38 µM	5.67
Ref. 71	3.7	NBT/ 250 µM	3.97
Ref. 72	0.96	WST / not reported	not reported
Ref. 73	18	NBT/ 56 µM	not reported
Ref. 74	50.14	NBT/ 56 µM	not reported
$(CuCl_2).6H_2O$*	1.62	NBT/ 38 µM	1.39

*use as control;

Table 4

Complex	V_{max} x 10^7 (mol L^{-1} s^{-1})	k_{cat} x10^3 (s^{-1})	K_m x 10^3 (mol L^{-1})	k_{cat}/K_m (L mol^{-1} s^{-1})
C1	1.26±0.08	4.73± 0.28	0.76± 0.18	6.62±1.55
C2	1.09± 0.15	4.08± 0.56	2.52± 0.88	1.62±0.61

C3	1.15± 0.02	4.33± 0.09	1.83± 0.11	2.37±0.15
C4	1.35± 0.09	5.06± 0.34	1.92± 0.37	2.63±0.53
C5	1.81± 0.04	6.78± 0.15	1.65± 0.11	4.11±0.15
Ref. [80]	-	0.83	1.2	0.69

Caption for figures

Figure 1. Molecular structure of the copper complex **C1** in a thermal ellipsoid representation with 40% thermal ellipsoids. Symmetry operations used to generate equivalent atoms: (#)2-*x*,-*y*, 1-*z*.

Figure 2. Molecular structure of the copper complex **C2** in a thermal ellipsoid representation with 40% thermal ellipsoids. Symmetry operations used to generate equivalent atoms: (#)2-*x*,-*y*, 2-z.

Figure 3. Molecular structure of the copper complex **C5** in a thermal ellipsoid representation with 40% thermal ellipsoids. Symmetry operations used to generate equivalent atoms: (#)-*x*, 2-*y*,1-*z*.

Figure 4. The CV of complexes **C1-C5**, using 0.1 M $TBAPF_6$ as support electrolyte and scan rate at 50 - 150 mV/s, respectively.

Figure 5. Plasmid DNA pBSK-II cleavage by complexes **(A)** complex **C1**, **(B)** complex **C2**, **(C)** complex **C3**, **(D)** complex **C4** and **(E)** complex **C5**. Reaction conditions: [DNA] = 330 ng, ~25 μM; [Buffer] = Hepes (10 mM, pH 7.0); [complex] = 10-250 μM; Temperature = 37 °C; Time = 16 hours sheltered from light. Results expressed as mean ± standard deviation of three independent tests.

Figure 6. Plasmid DNA pBSK-II cleavage by complexes **(A)** complex **C1**, **(B)** complex **C2**, **(C)** complex **C3**, **(D)** complex **C4** and **(E)** complex **C5** in the presence of different DNA groove blockers netropsin (Net) and methyl green (VM). Reaction conditions: [DNA] = 330 ng, ~25 μM; [Buffer] = Hepes (10 mM), pH 7.0; [complex] = 250 μM; [Net] or [VM] = 50 μM; Temperature = 37 °C; Time = 16 hours sheltered from light. Results expressed as mean ± standard deviation of three independent tests.

Figure 7. Plasmid DNA pBSK-II cleavage by complexes **(A)** complex **C1**, **(B)** complex **C2**, **(C)** complex **C3**, **(D)** complex **C4** and **(E)** complex **C5** in the presence of different reactive oxygen species scavengers potassium iodate (KI) and sodium azide (NaN_3). Reaction conditions: [DNA] = 330 ng, ~25 μM; [Buffer] = Hepes (10 mM, pH 7.0); [complex] = 250 μM; [KI] or [NaN_3] = 0.5 mM; Temperature = 37 °C; Time = 16 hours sheltered from light. Results expressed as mean ± standard deviation of three independent tests.

Figure 8. Neperian logarithm graph of supercoiled plasmid DNA *versus* reaction time (hours) after the treatment with complexes **(A)** complex **C1**, **(B)** complex **C2**, **(C)** complex **C3**, **(D)** complex **C4** and **(E)** complex **C5**. Reaction conditions: [DNA] = 330 ng, ~25 μM; [Buffer] = Hepes (10 mM, pH 7.0); [complex] = 250 μM (except complex **C5** = 50 μM); Temperature = 37 °C; Time = 0 to 24 hours sheltered from light. Results expressed as mean ± standard deviation of three independent tests.

Figure 9. Graph of initial velocities of V_o *versus* pH to the oxidation reaction of the substrate 3,5-DTBC catalyzed by complexes **C1** to **C5** in MeOH/H_2O/DMSO mixture (38:1:1) at 25 ºC under the following conditions: $[C]_{Final}$ = 2 x 10^{-5} mol/L in DMSO; $[3,5\text{-DTBC}]_{Final}$ = 2.5 x 10^{-3} mol/L in MeOH; $[buffer]_{final}$ = 0.1 mol/L without ionic strength in H_2O (**9A**). Graph of initial velocities of V_o *versus* the substrate concentration for the hydrolysis reaction of 3,5-DTBC at pH 6.44 catalyzed by complexes **C1** to **C5** in MeOH/H_2O/DMSO (38: 1: 1) at 25 ° C under the following conditions: $[C]_{Final}$ = 5 x 10^{-5} mol/L in DMSO; $[3,5\text{-DTBC}]_{Final}$ = 5 x 10^{-4} to 7.5 x 10^{-3} mol/L in MeOH; $[buffer]_{final}$ = 0.1 mol/L without ionic strength in H_2O (**9B**).

Figure 1

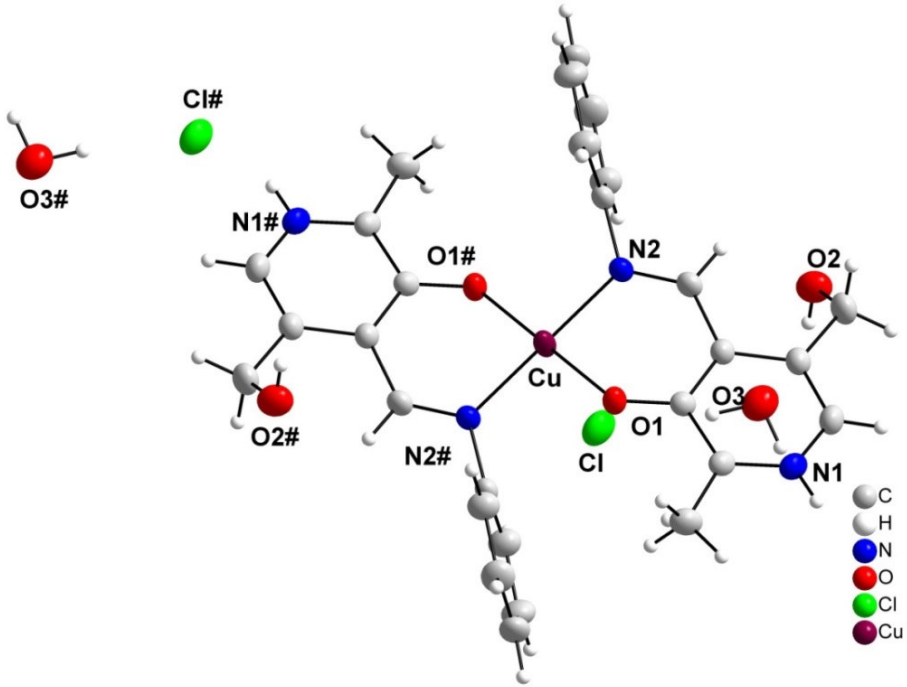

Figure 2

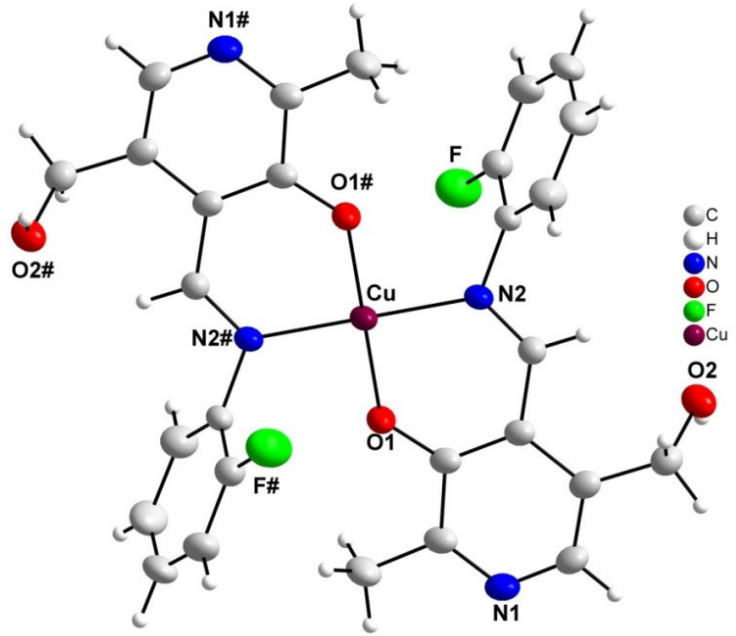

Figure 3

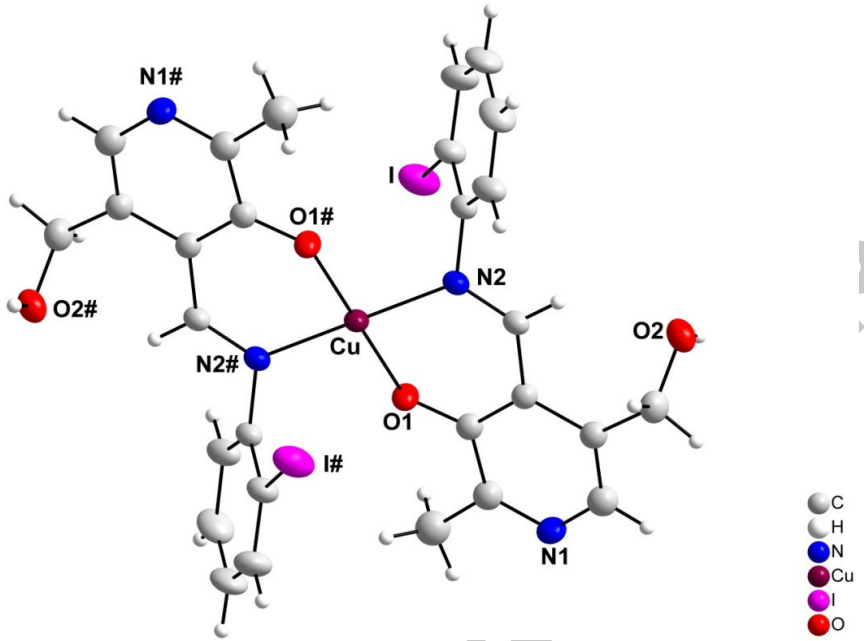

Figure 4

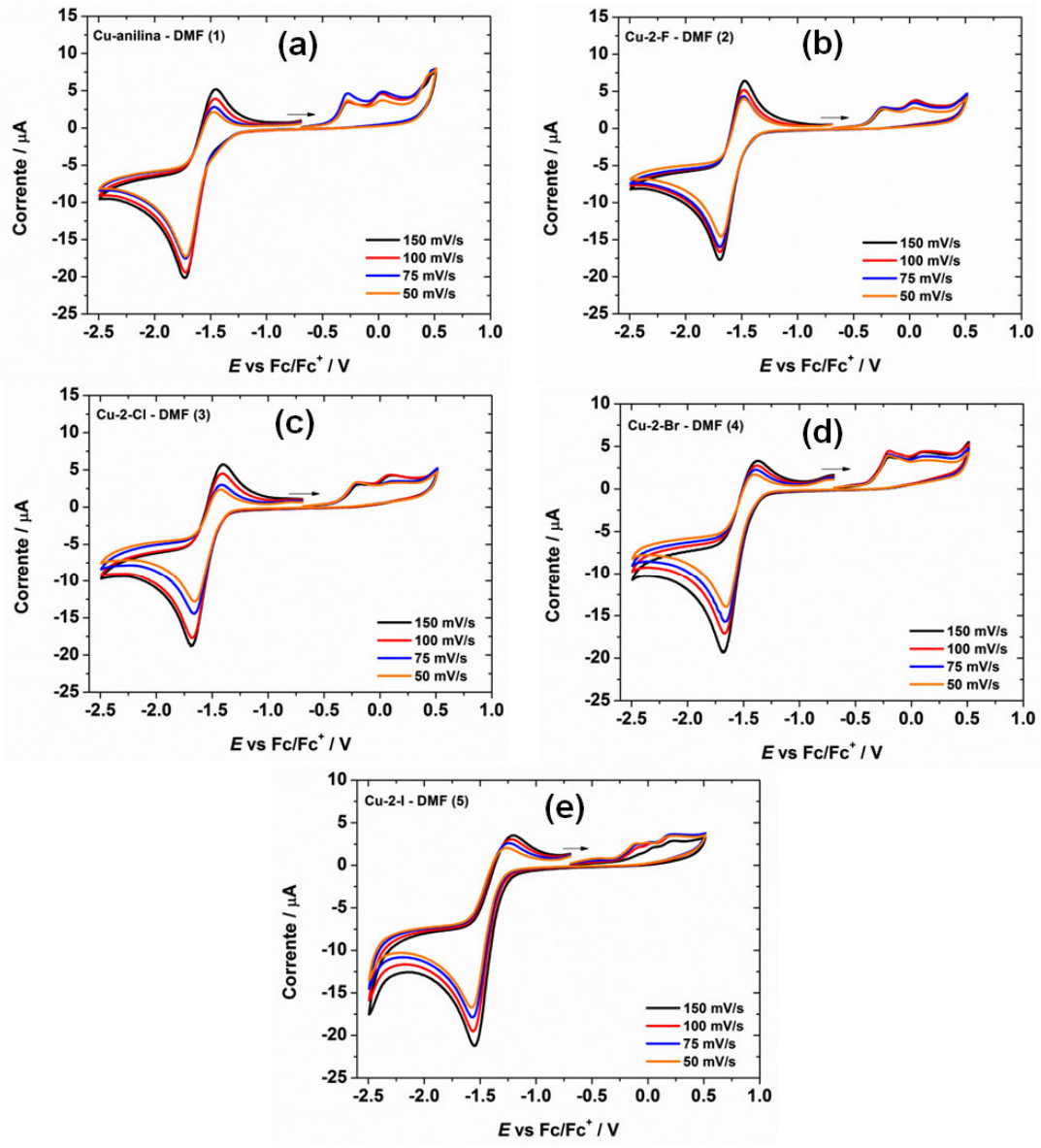

Figure 5

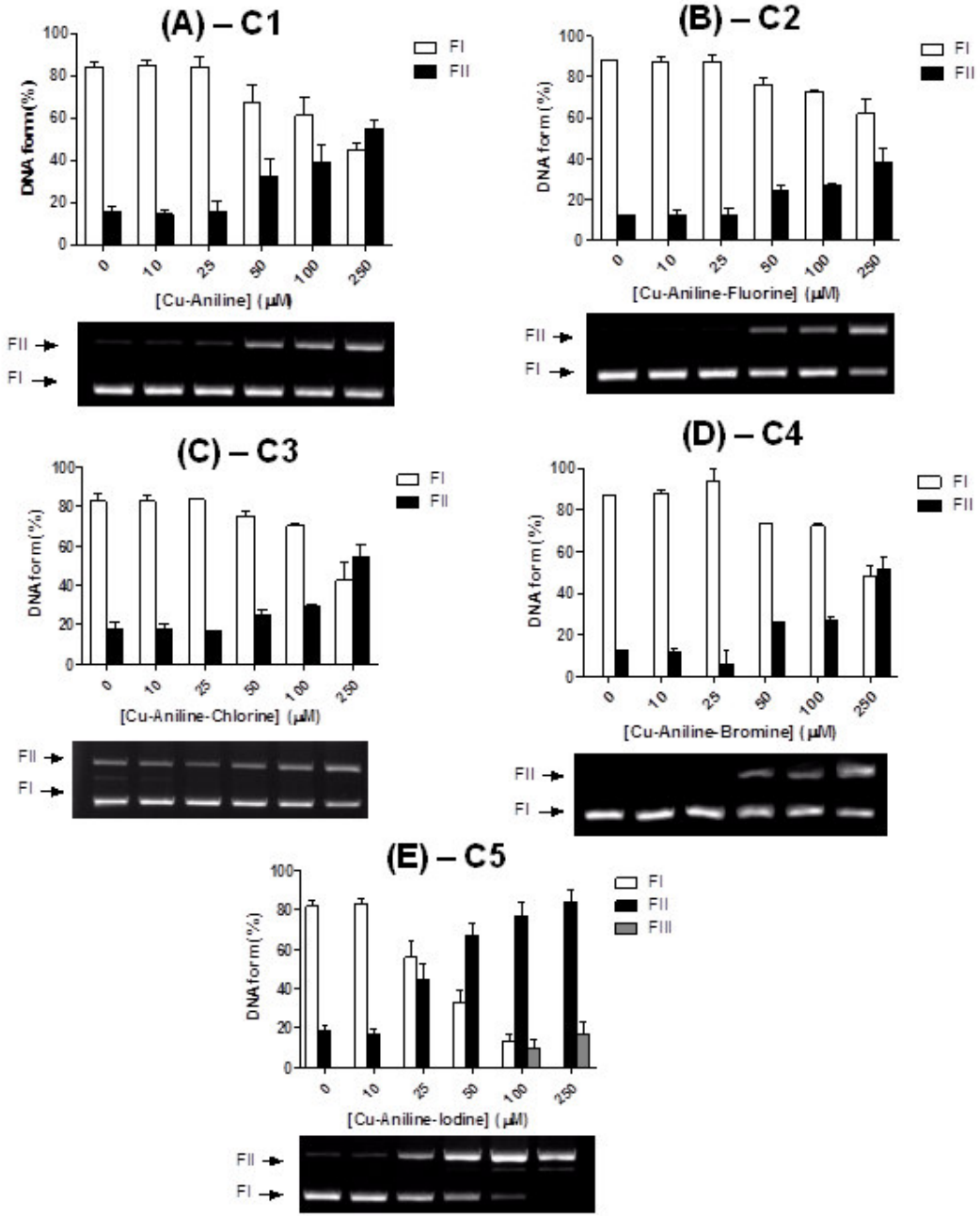
(A) – C1
DNA form(%)
FI
FII
[Cu-Aniline] (μM)
(B) – C2
[Cu-Aniline-Fluorine] (μM)
(C) – C3
[Cu-Aniline-Chlorine] (μM)
(D) – C4
[Cu-Aniline-Bromine] (μM)
(E) – C5
FIII
[Cu-Aniline-Iodine] (μM)

Figure 6

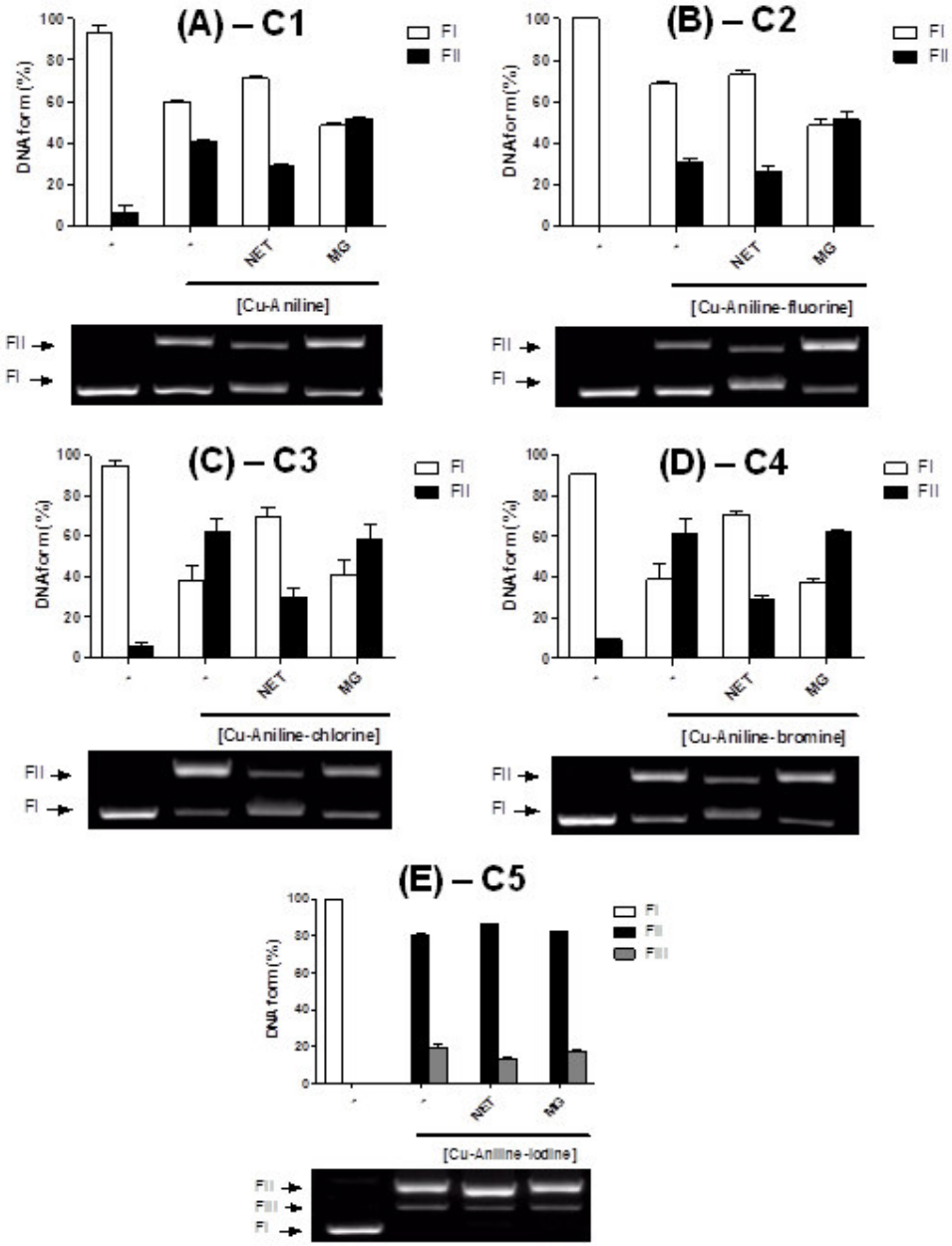

Figure 7

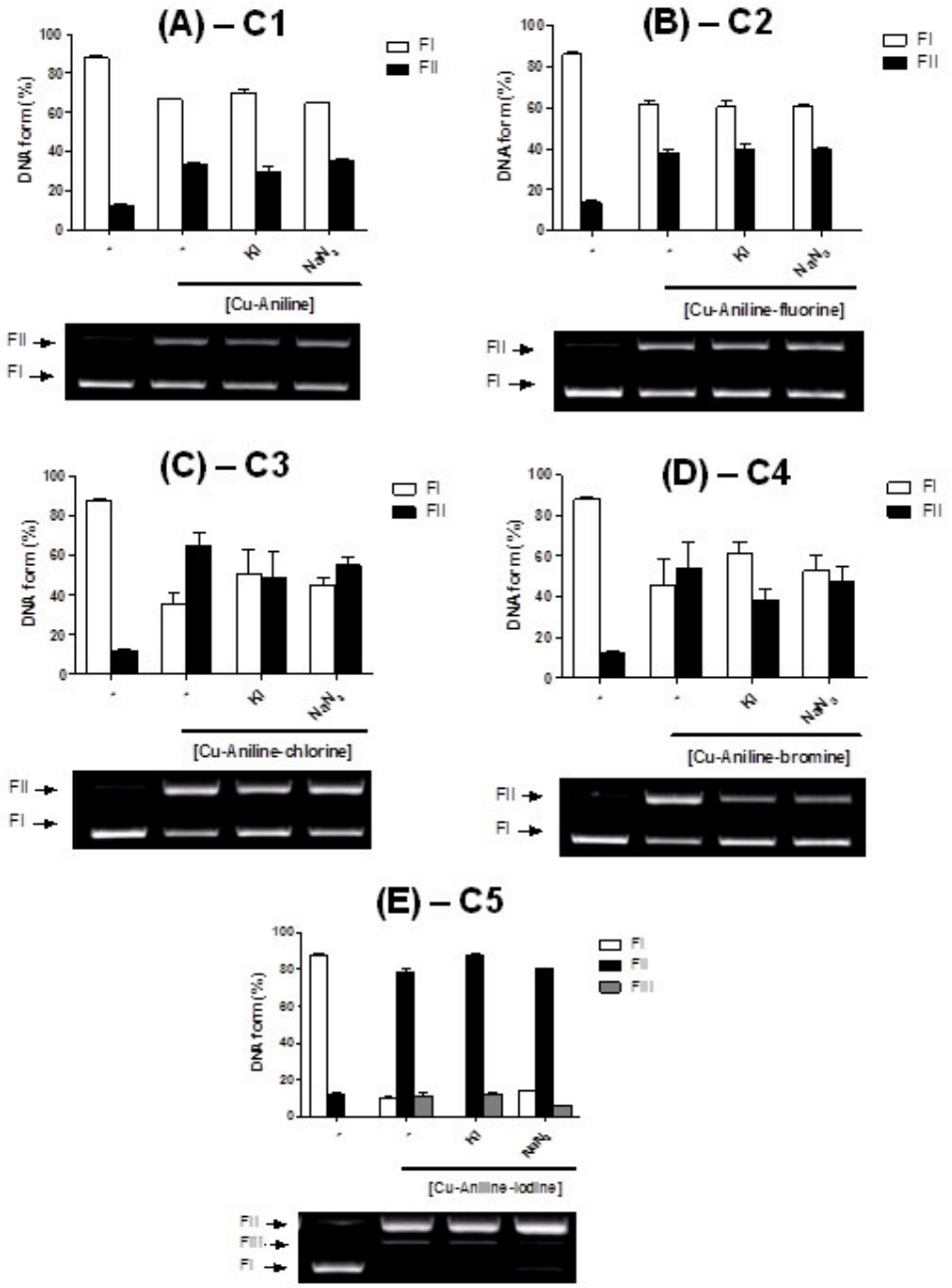

Figure 8

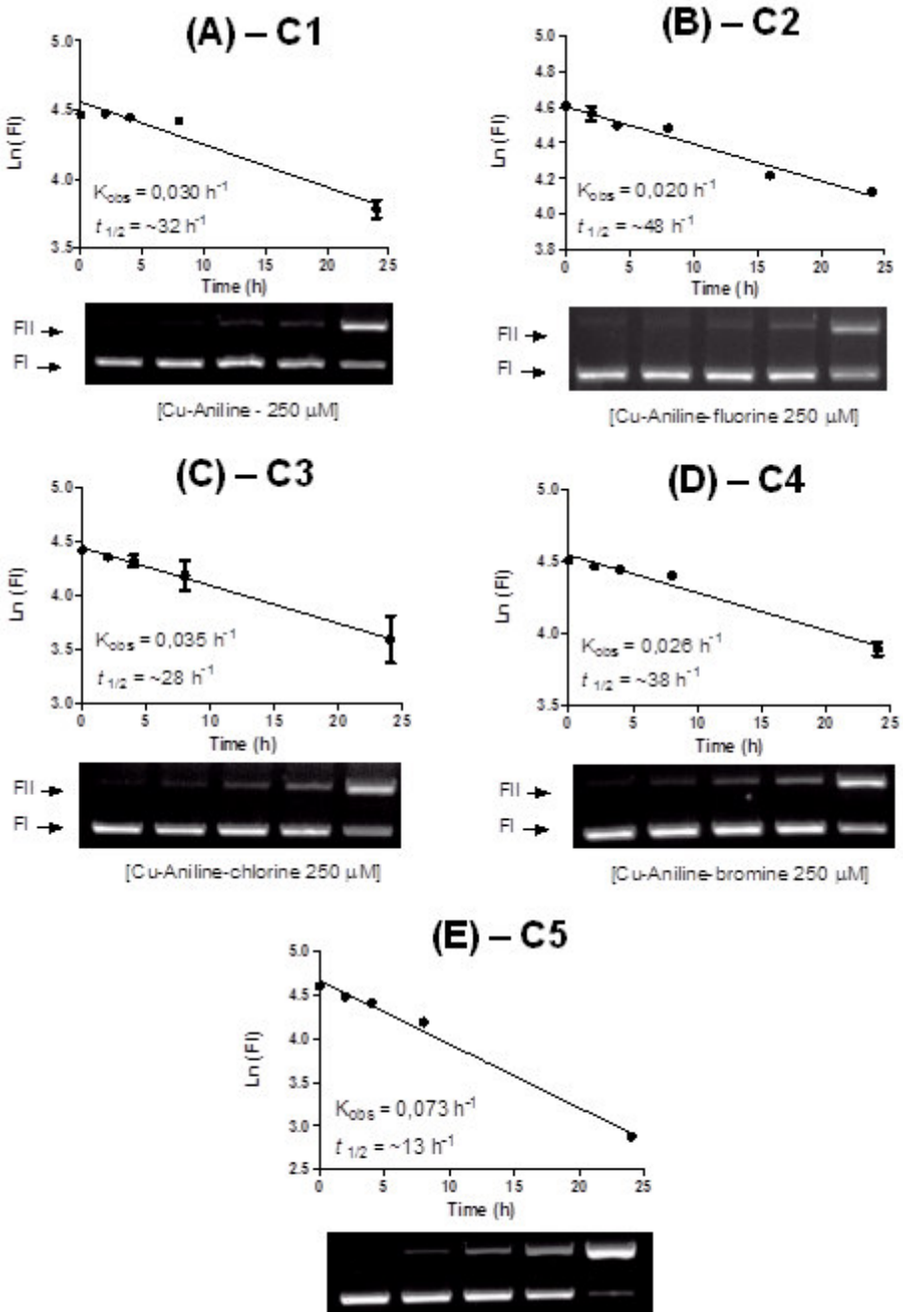

Figure 9 (9A and 9B)

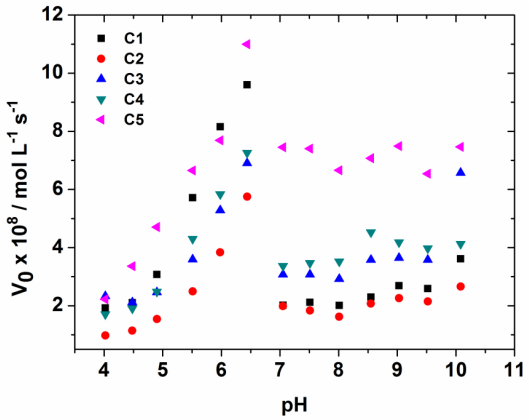

9A

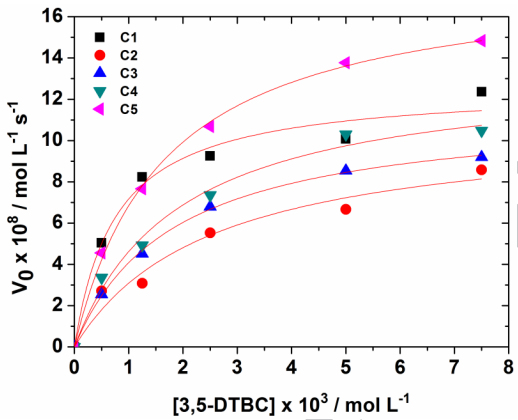

9B

Copper (II) Schiff bases complexes derived from condensation of pyridoxal and ortho-halogenated substituted anilines were versatile mimetic of SOD.

All complexes was evaluated by the oxidation reaction using 3,5-ditert-butylcatechol as substrate (3,5-DTBC) and as agents for DNA cleavage.

The complex 5 showed a high antioxidant activity against the inhibition of superoxide ions. As for catecholase activity, complex 5 also showed better activity, but lower, if compared to literature data.

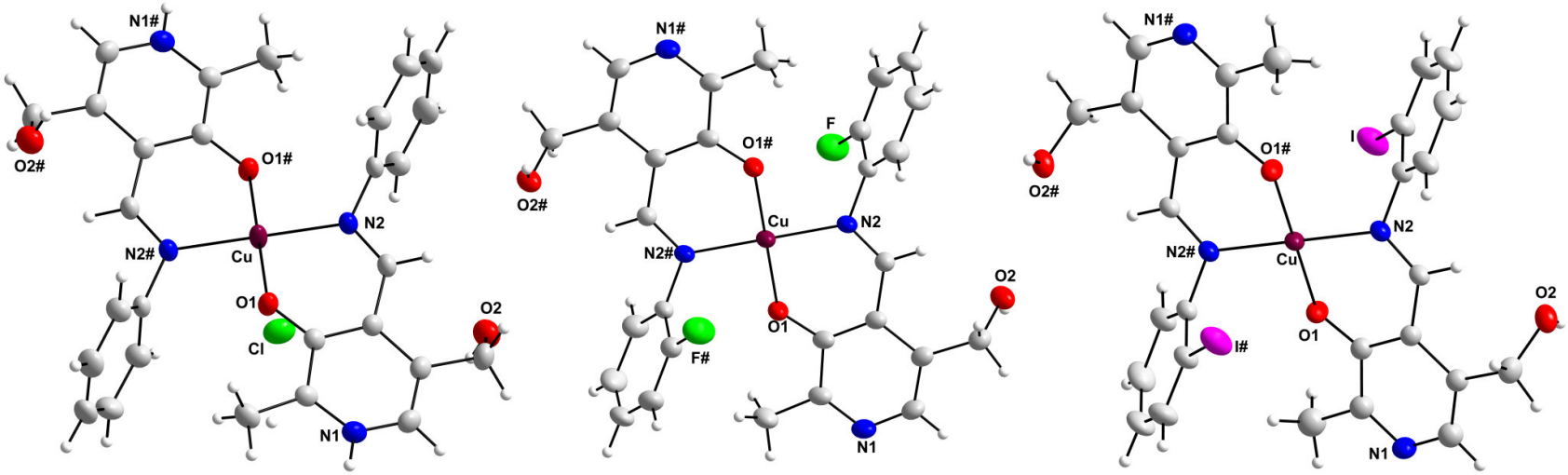

DNA CLEAVAGE

SUPEROXIDE DISMUTASE ACTIVITY

CATECHOLASE ACTIVITY